SYNTHESIS AND CHARACTERIZATION OF OXIDE NANOPARTICLES FOR ITS APPLICATION IN MEMRISTIVE DEVICES

Jyoti Prasad Roy Choudhury[*a,b], Barnali Pathak[a], Nayan Mani Nath[c], and Bikash Borah[b]

[a]*Department of Physics, B.H.College, Howly, 781316, Assam, India*
[b]*Department of Physics, Assam Don Bosco University, Sonapur, 784028, Assam, India*
[c]*Department of Physics, Barnagar College, Sorbhog, 781317, Assam, India*

[*]Corresponding Author: jyotirc62@gmail.com

(Received 6 September 2025; revised 12 November 2025; accepted 17 November 2025; published 6 April 2026)

Abstract: Zinc and lead oxide (ZnO & PbO) nanoparticles synthesis was carried out using a low-cost chemical precipitation technique with polyvinylpyrrolidone (PVP) as the stabilizer. These semiconducting metal oxides were chosen because of their distinct electronic characteristics and their wide applications in upcoming generation as memory devices. Structural and morphological analyses were carried out using XRD and HRTEM study, verifying the formation of crystalline ZnO with a hexagonal wurtzite structure and PbO with an orthorhombic phase. The average crystallite sizes were calculated and found to be approximately 28.93 and 63.11 nm for ZnO and PbO respectively, indicating successful nanoscale synthesis. Electrical characterization was performed using a planar electrode configuration and a Keithley 2450 SourceMeter to evaluate the current-voltage (VI) behavior. Both samples exhibited a prominent zero-crossing pinched hysteresis loop in their VI curves which is a hallmark of a pure memristive behavior. The switching between High and Low Resistance State i.e. HRS and LRS respectively is governed by SET and RESET voltages, was stable and repeatable across multiple cycles, demonstrating strong potential for non-volatile memory applications. The results suggest that ZnO and PbO thin films can act as reliable memristive elements capable of storing and retaining binary information. Their stable resistive switching behavior makes them promising candidates for use in resistive random-access memory (RRAM) and neuromorphic computing systems. This work not only validates the memristive properties of these materials but also paves the way for their integration into low-cost, high-performance electronic devices.

Keywords: Zinc Oxide, Lead Oxide nanoparticles, opto-electronics behavior, memristivity, pinched hysteresis curve.

PACS: 81.05.Hd

1 Introduction

For the past several years, metal oxide semiconductor nanoparticles have attracted significant research interest due to their remarkable physicochemical properties. These include tunable electrical conductivity, a high surface area with respect to its volume, and pronounced quantum confinement effects, which make them highly suitable for various advanced applications in almost every field. Among several nanoparticles, zinc oxide (ZnO) and lead oxide (PbO) stand out due to their distinct electronic characteristics. ZnO possesses a wide band gap of approx 3.37 eV and also exhibits a high exciton binding energy of nearly 60 MeV, which makes it particularly advantageous for optoelectronic and photonic devices [1]. On the other hand, the band gap of PbO is comparatively narrower which is about 2.59 eV [2] at room temperature, making it suitable for different applications that require lower energy thresholds. ZnO, in particular, is extensively utilized in biomedical and environmental fields because of its non-toxic, biocompatible, and eco-friendly nature, making it a widely available and versatile material [3].

The concept of memristive behavior in semiconducting materials was first introduced by Leon Chua in 1971, who theoretically proposed the presence of a fourth essential circuit element known as memristor alongside the well-established resistor, capacitor, and inductor [4]. The memristor, short for "memory resistor," is a device with two terminals that directly relates electric charge with magnetic flux [5]. Its key feature is its ability to retain information about the amount of electrical current that has previously passed through it. This non-volatile memory behavior helps the memristor to "remember" the most recent resistance that passed through it even after the power is turned off, making it a promising candidate for future memory storage and neuromorphic computing technologies [6, 7].

A significant breakthrough in this area came in 2008 as the scientists at HP Labs perform their first experiment that validate Chua's theoretical model by demonstrating memristive behavior in a thin film of titanium dioxide (TiO_2) [6]. Since then, the field has witnessed a surge in studies exploring memristive effects in various nanomaterials and metal oxide-based systems. In particular, oxide-based nanocomposites have been the subject of extensive investigation due to their stable and reproducible electrical switching characteristics. The VI characteristic of these materials shows a zero crossing pinched hysteresis curve, which is a signature of memristive behavior [8, 9]. In our study, the fabricated samples also demonstrated such a loop, indicating the presence of memristive properties.

Numerous researchers have explored similar findings across different material systems [10]. For example, in a study conducted by Barnes $et.al$ and colleagues during 2018, a ZnO-based memristor exhibited a clear hysteresis loop within a voltage sweep range of +20V to -20V, further confirming the suitability of ZnO in memristive device applications [11]. These findings highlight the potential of metal oxide nanostructures, particularly ZnO, as promising candidates for next-generation memory and logic devices, paving the way for advancements in nanoelectronics and artificial intelligence hardware.

In recent years, extensive research has been carried out on ZnO and PbO nanoparticles across various fields. However, the available studies remain inadequate for developing memristive devices that effectively utilize their promising optoelectronic properties. To bridge this research gap, ZnO and PbO nanoparticles were prepared by a simple and inexpensive chemical bath deposition technique, employing a PVP matrix to regulate particle growth. Although numerous studies have explored oxide-based nanocomposites, reports focusing specifically on the memristive behavior and its sensitivity $i.e.$ the Roff/Ron ratio of ZnO and PbO nanoparticles are lacking.

Unlike previous works that utilized complex and expensive synthesis methods for other oxide nanomaterials, this study demonstrates that ZnO and PbO nanoparticles, prepared through a straightforward and low-cost process, exhibit notable memristive properties. The structural, electrical, and morphological characteristics of these samples are analyzed and correlated with their mem-behavior, offering valuable insights for the design and development of next-generation mem-devices.

2 Synthesis of ZnO and PbO Nanoparticles

All the chemical reagents required for our experimental procedures were procured from Merck to ensure analytical-grade purity. The primary chemicals utilized in the synthesis process included Zinc Acetate Di-hydrate having chemical formula $Zn(CH_3COO)_2 \cdot 2H_2O$, Lead Acetate $i.e.$ $Pb(CH_3COO)_2 \cdot 4H_2O$, Sodium Hydroxide $i.e.$ NaOH & Polyvinylpyrrolidone which is PVP, which was used as a stabilizing and capping agent. To prepare the necessary reaction medium, a 3% PVP liquid solution was first made by adding an appropriate amount of PVP powder mixed in distilled water under constant magnetic stirring to ensure complete homogenization.

2.1 Production of ZnO Nanoparticles

To synthesize ZnO nanoparticles, a 0.3 M solution of $Zn(CH_3COO)_2 \cdot 2H_2O$ was made by dissolving Zn-salt into 50 mL of the preprepared 3% PVP solution at room temperature. The solution was stirred continuously until the Zinc Acetate was completely dissolved and uniformly dispersed in the polymer matrix. Once a clear and homogenous solution was obtained, 1 M of NaOH (50 mL) is added in drops to the solution maintaining the reaction temperature at approximately $90^{\circ}C$. This addition was performed under continuous stirring to ensure controlled formation and development of the nanoparticles. After about 45 to 50 minutes of reaction time, the solution gradually turned milky white, which is a visual indication of the successful formation of ZnO nanoparticles. The resulting colloidal solution was then subjected to filtration to separate the solid product. The collected precipitate was subsequently dried in a hot air oven to remove residual moisture and obtain the dry ZnO nanopowder.

2.2 Production of PbO Nanoparticles

PbO nanoparticles were also prepared following a similar process. A solution of 0.3 M of $\mathrm{Pb(CH_3COO)_2 \cdot 4H_2O}$ was made by mixing the appropriate amount of Pb-salt in 50 mL PVP (3%) at ambient temperature. The solution was stirred until the salt was completely dissolved and uniformly incorporated into the PVP medium. Now, 50 mL of 1 M NaOH solution is introduced slowly in the reaction medium in a dropwise manner, while maintaining the system at $90^{\circ}C$ under vigorous stirring. Over a period of approximately 60 to 70 minutes, the solution began to change color from colorless to a pale yellow hue, signifying the formation of PbO nanoparticles. Following this color change, the reaction mixture was filtered to isolate the solid PbO product. The filtered nanoparticles were then dried in a hot air oven to remove any remaining moisture, yielding the final PbO nanopowder.

This synthesis approach, utilizing PVP as a stabilizing agent, helps in controlling the particle size and preventing agglomeration during the formation process. Both ZnO and PbO nanoparticles produced through this method were later used for further characterization and device fabrication studies.

2.3 Characterization Techniques

A variety of advanced techniques for characterization were employed that analyze the properties such as: structural properties, morphological properties, and electrical properties of the synthesized semiconducting nanomaterials. These techniques play a crucial role in determining key parameters such as crystal structure, particle size, surface morphology, elemental composition, and optical and electrical behavior. Among the methods used, XRD, HRTEM, and electrical characterization done using precision electrometers were central to our study.

The investigation of the crystallographic structure and also to study the purity phase of the prepared nanoparticles, XRD analysis was done using an ULTIMA IV X-Ray diffractometer. This technique gives all the information about the crystal system, lattice parameters, and average crystallite size through analysis of diffraction patterns. The XRD peaks also confirm the crystalline nature and formation of ZnO and PbO nanoparticles by studying the sharpness and intensity of the peaks.

For further insights into the microstructure and morphology study, HRTEM was utilized. This technique enabled visualization of the shape, size distribution, and particle boundaries with high spatial resolution. HRTEM also provided detailed lattice fringe images that is use to support the crystalline structure and to measure interplanar spacing, thereby validating the results obtained from XRD analysis.

2.4 Electrical Characterization

The electrical behaviors of the synthesized samples were analyzed using a Source-Meter, which allowed precise VI measurements. A planar electrode configuration with a defined gap was utilized for I-V measurement. The prepared sample is placed between two silver electrodes (Ag paste) which is finally placed in a glass substrate. Both the electrodes are then connected to a computer interfaced Keithley-2450 electrometer source for the measurement of required electrical data. The electrical response of the samples was measured by sweeping the voltage between –10V +10V. These VI measurements were critical in evaluating the memristive behavior of the samples and in identifying non-linear and hysteretic behavior in the current-voltage relationship, which is indicative of memory-resistance character.

Thus all these techniques gives a detail comprehensive understanding of all the structural and functional properties of the prepared ZnO and PbO nanomaterials, enabling further evaluation of their potential in memristive and other electronic applications.

3 Results and Discussion

Structural analysis of the as prepared ZnO and PbO semiconductor nanoparticles were thoroughly investigated with the help of X-ray Diffraction (XRD) analysis. This technique is essential for determining the crystallographic structure, lattice parameters, and average crystallite size of nanomaterials. The famous Bragg's Law is the basic principle behind XRD analysis, that relates the angle of diffraction to the interplanar spacing in a crystalline material [12, 13]. The Bragg equation is expressed as:

$$2d \sin\theta = n\lambda \tag{1}$$

Where,

λ known is wavelength of the X-ray beam used whose value is 1.5406 Å,
θ known as angle of diffraction,
d is called interplanar spacing, and
The diffraction order is used as n (taken as 1 for simplicity).

Upon analyzing the XRD spectra of the prepared samples Fig. 1, distinctive diffraction patterns were observed, confirming the crystalline nature of both ZnO and PbO nanoparticles. According to standard reference data from the JCPDS- 00 001 1136 and JCPDS- 00 003 0599, the diffraction peaks for ZnO correspond well with a hexagonal wurtzite crystal structure, while those for PbO match an orthorhombic structure respectively.

For ZnO nanoparticles, characteristic peaks were identified at the planes (100), (002), (101), and (110), indicative of a hexagonal phase. For PbO nanoparticles, the diffraction peaks observed at (002), (201), (003), and (131) confirm the orthorhombic crystalline phase. These observations validate the successful formation of the desired crystalline structures for both materials.

Using the peak positions from the XRD patterns, the lattice constants were calculated. Lattice parameters of ZnO were found to be 3.238 & 5.200Åwhich are consistent with standard values for hexagonal ZnO structures. Whereas for PbO nanoparticles, the parameters were found to be 5.49, 4.73 & 5.86Åconfirming orthorhombic phase of PbO. To estimate the crystallite dimension, Debye–Scherrer formula was applied:

$$D = \frac{K\lambda}{\beta \cos\theta} \tag{2}$$

Where,
D known as crystallite dimension,
K is known as the shape factor whose value is 0.9,
λ known as X-ray wavelength (1.5406 Å),
β known as FWHM of diffraction peak (in radians), &
θ is known as the Bragg angle.

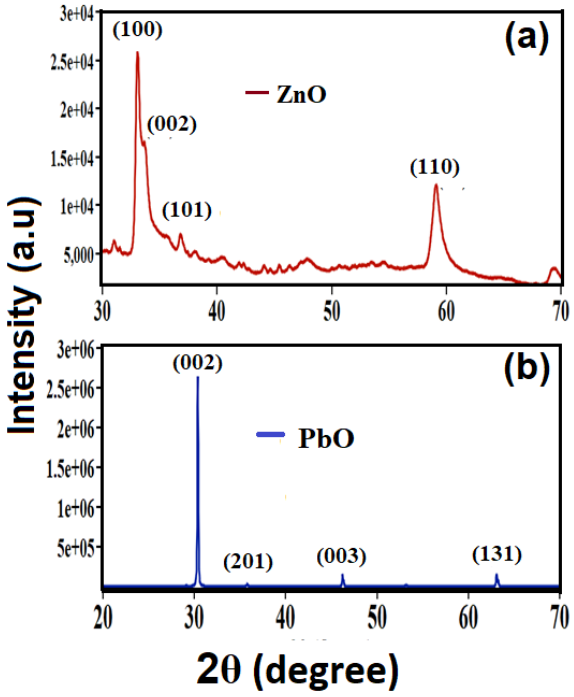

Figure 1: XRD pattern observed for prepared ZnO and PbO

Using this equation, the crystallite sizes of the synthesized nanoparticles were calculated. The crystallite dimension (size) was found to be approximately 28.93 and 63.11 nm for ZnO and PbO respectively, suggesting that the ZnO nanoparticles are finer and more narrowly distributed compared to PbO. These structural findings derived from XRD analysis established the successful formation of the crystalline ZnO and PbO nanomaterials

with their respective lattice structures and nanoscale dimensions. Detailed XRD data, including diffraction angles, FWHM, and size, are summarized in the table below.

Sample	2θ (degree)	FWHM	Size (nm)	Average size (nm)
ZnO	33	0.307	26.38243	28.934
	35.79	0.358	22.79518	
	38.1	0.409	20.08757	
	56.705	0.170	46.4701	
PbO	30.69	0.1535	52.00127	63.110
	36.343	0.1023	76.57744	
	46.535	0.1279	61.45046	
	63.204	0.1223	62.41900	

Table 1: Data obtained from XRD study

The structural and surface morphological features of the synthesized ZnO and PbO nanoparticle samples were thoroughly investigated using HRTEM. The micrographs, are shown in Fig. 2, clearly reveal that the ZnO nanoparticles exhibit a well-defined structure. This is evident from the uniform and periodic lattice fringes observed in the images. On the other hand, the PbO particles demonstrate a distinct morphology. These morphological features are consistent with the structural patterns observed in the XRD analysis, confirming the phase purity and crystallinity of the synthesized materials.

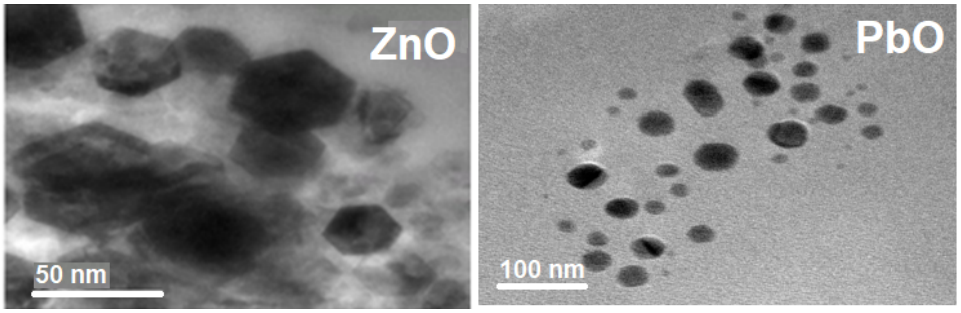

Figure 2: HRTEM images for ZnO and for PbO nanomaterials of different magnifications

A planar electrode configuration with a defined gap was utilized to investigate the VI graph of the thin film. This geometry allows for precise measurement of electrical behavior across the sample. The VI measurements are done by using a Keithley 2450 Source-Meter electrometer, which is well-suited for sourcing voltage and measuring the resulting current with high accuracy and sensitivity. This instrument enabled detailed analysis of the electrical response of the material under study. To aid in understanding the experimental setup, a simplified schematic diagram illustrating the measurement arrangement with the Keithley 2450 electrometer is presented below in Fig. 3. This setup ensures a good and reproducible technique for characterizing the electrical properties of thin films using the gap-type planar electrode structure.

The VI characteristic graph for both nanoparticles were plotted over a voltage range from -10V – +10V as shown in Fig. 4(a&b). These curves provide insight into the electrical behavior and conduction mechanisms of the materials under the applied voltage. The resulting plots, shows zero crossing hysteresis graph which is the prime characteristic of a memristor. This confirms that our prepare device can acts as a memristor.

4 Memristive Behavior of prepared nanoparticles

The VI characteristics obtained from the prepared samples demonstrate a distinct zero-crossing pinched hysteresis loop, a well-known and defining feature of memristive systems [14]. This pinched hysteresis behavior, where the I-V curve intersects the origin: is considered a key indicator of memristive functionality. In the context of our study, the loops observed clearly confirm the memristive nature of the devices, with the point of intersection (pinching) occurring precisely at the origin of the current-voltage plane.

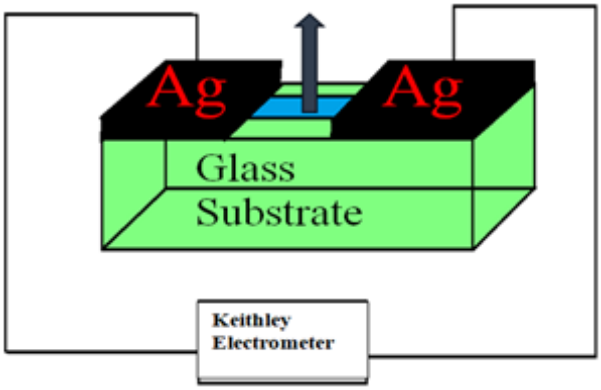

Figure 3: Electrical measurement done using source meter

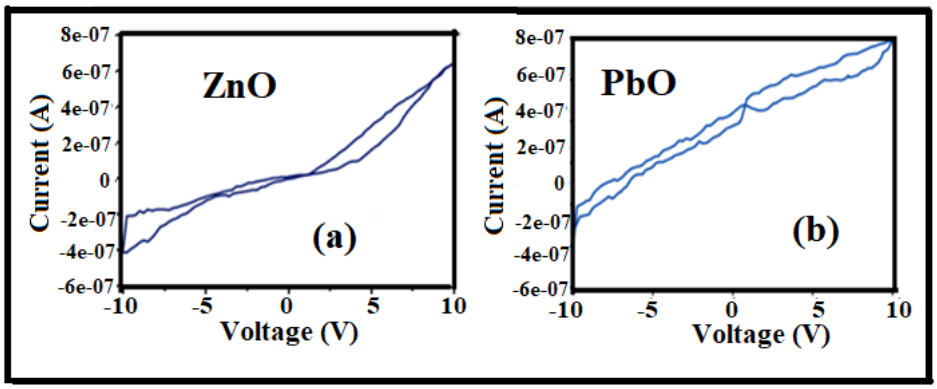

Figure 4: (a) VI graph of ZnO & (b) PbO

As shown in Fig. 5, the measurement sequence was carefully designed to observe this behavior. The voltage was swept in four stages: from 0 V t→ +10 V → 0 V → -10 V → 0 V. During the initial increase from 0 V → +10 V, the current in the device gradually increased, indicating that the device initially to be at in a High Resistance State (HRS). As the voltage reached around +10 V, a transition occurred that shift the device into the Low Resistance State (LRS), also referred to as the ON state. This voltage threshold at which the device goes from HRS to LRS is known as the SET voltage [15].

Once in the LRS, the device maintained this state as the voltage was swept toward the negative range. Upon reaching approximately -10 V, another transition was observed—this time from LRS back to HRS—marking the device's return to the OFF state. The voltage at which this transition occurs is termed the RESET voltage [16].

To give a clear picture of this resistive switching behavior, a representative I-V plot is included in Fig. 5, illustrating the change between HRS and LRS states. Multiple measurements were conducted to ensure the reliability of the obtained results. Across several cycles, the same pinched hysteresis pattern was consistently observed in both ZnO and PbO thin film-based memristive devices. This repeatability strongly suggests stable switching characteristics and reliable memristive behavior in the fabricated devices.

The zero-crossing pinched hysteresis loop typically consists of two distinct states: the LRS and the HRS. This state gives the fundamental switching behavior of memristive devices. The transition from HRS to LRS and from LRS back to HRS is crucial for memory-related applications, as it enables the storage and retrieval of binary information. This switching capability forms the basis for employing memristors in non-volatile memory technologies, where the two resistance states correspond to logical "0" and "1", thereby highlighting their potential in next-generation memory and neuromorphic computing systems.

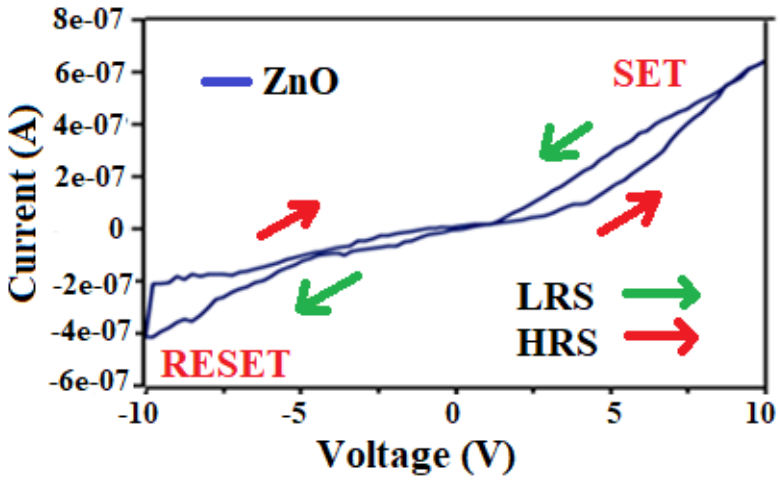

Figure 5: Zero crossing behavior of memristor with arrow indicating the direction of current.

5 Conclusion

Thus this study explains the preparation, characterization, and electrical behavior of ZnO and PbO nanoparticles, with a particular focus on their memristive properties. Using a straightforward chemical precipitation method aided by polyvinylpyrrolidone (PVP) as a stabilizing agent, both ZnO and PbO nanoparticles were synthesized under controlled conditions. The synthesis route proved effective in producing nanomaterials with desired phase purity, morphology, and crystallinity. Structural and morphological analysis confirmed the successful formation of the respective crystal structures—hexagonal wurtzite for ZnO and orthorhombic for PbO—as evidenced XRD and HRTEM. The crystallite dimension, calculated using the D-S equation, was found to be in the nanoscale range, approximately 28.93 and 63.11 nm for ZnO and PbO respectively. These findings affirm that the synthesis method employed was suitable for producing well-defined, nanosized semiconducting metal oxide particles. Electrical characterization was conducted using a gap-type planar electrode configuration in combination with a Keithley 2450 Source-Meter, allowing accurate VI measurements. Both ZnO and PbO thin films exhibited a clear zero-crossing pinched hysteresis loop in their I-V curves, which is a hallmark of memristive behavior. These loops indicate a reversible transition between a HRS and LRS, governed by SET and RESET voltages. The observed resistive switching behavior confirms the potential of these materials for application in non-volatile memory devices. Furthermore, the memristive characteristics showed good repeatability over multiple voltage cycles, demonstrating the devices' stability and consistency. This repeatable hysteresis loop implies that both ZnO and PbO thin films possess the essential features required for use in resistive random-access memory (RRAM) and neuromorphic systems, where the ability to switch and retain resistance states is critical. In summary, this work highlights the feasibility of using chemically synthesized ZnO and PbO nanoparticles in memristive device applications. Their favorable electrical behavior, combined with structural and morphological integrity, opens up promising avenues for their integration into future memory storage technologies and next-generation intelligent computing architectures.

Acknowledgement

We would like to thank SAIF Gauhati University for providing XRD facility, Department of Physics, Gauhati University and CIF IIT Guwahati for HRTEM facility.

References

[1] S. S. Kumar, P. Venkateswarlu, V. R. Rao, and G. N. Rao, International Nano Letters **3**, 30 (2013).

[2] D. H. Besisa, E. M. Ewais, and Y. M. Ahmed, Journal of Environmental Management **285**, 112094 (2021).

[3] H. Mirzaei and M. Darroudi, Ceramics International **43**, 907 (2017).

[4] T. Dao Thanh, V.-T. Pham, and C. Volos, in *Mem-elements for Neuromorphic Circuits with Artificial Intelligence Applications*, Advances in Nonlinear Dynamics and Chaos (ANDC), edited by C. Volos and V.-T. Pham (Academic Press, 2021) pp. 347–360.

[5] L. Chua, IEEE Transactions on Circuit Theory **18**, 507 (1971).

[6] D. B. Strukov, G. S. Snider, D. R. Stewart, and R. S. Williams, Nature **453**, 80 (2008).

[7] L. Wang, C. Yang, J. Wen, S. Gai, and Y. Peng, Journal of Materials Science: Materials in Electronics **26**, 4618 (2015).

[8] B. Pathak, P. Kalita, N. M. Nath, N. Aomoa, and J. Choudhury, Materials Science in Semiconductor Processing **149**, 106892 (2022).

[9] D. Yu, Y. Liang, H. H. C. Iu, and L. O. Chua, IEEE Transactions on Circuits and Systems II: Express Briefs **61**, 758 (2014).

[10] F. Gul and H. Efeoglu, Ceramics International **43**, 10770 (2017).

[11] B. K. Barnes and K. S. Das, Scientific Reports **8**, 2184 (2018).

[12] P. A. Rundquist, P. Photinos, S. Jagannathan, and S. A. Asher, The Journal of Chemical Physics **91**, 4932 (1989).

[13] V. D. Mote, Y. Purushotham, and B. N. Dole, Journal of Theoretical and Applied Physics **6**, 6 (2012).

[14] Y. V. Pershin and M. Di Ventra, Journal of Physics D: Applied Physics **52**, 01LT01 (2018).

[15] Y. Yu, C. Wang, C. Jiang, I. Abrahams, Z. Du, Q. Zhang, J. Sun, and X. Huang, Applied Surface Science **485**, 222 (2019).

[16] T. D. Dongale, P. J. Patil, N. K. Desai, P. P. Chougule, S. M. Kumbhar, P. P. Waifalkar, P. B. Patil, R. S. Vhatkar, M. V. Takale, P. K. Gaikwad, and R. K. Kamat, Nano Convergence **3**, 16 (2016).